Springer

KSME

Journal of Mechanical Science and Technology 30 (9) (2016) 4239~4246
www.springerlink.com/content/1738-494x(Print)/1976-3824(Online)
DOI 10.1007/s12206-016-0836-8

Numerical simulation of fluid flow and forced convection heat transfer around a circular cylinder with control rods located in equilateral triangular arrangement †

Somayeh Harimi[1], Azam Marjani[1,*] and Sadegh Moradi[2]

[1]*Department of Chemistry, Arak Branch, Islamic Azad University, Arak, Iran*
[2]*Department of Chemical Engineering, Arak University, Arak, Iran*

(Manuscript Received February 2, 2016; Revised April 20, 2016; Accepted May 1, 2016)

Abstract

Numerical study of forced convection heat transfer and fluid flow in laminar flow regime for a circular cylinder attached by three control rods is performed using the overset grid method. The aim of this work is evaluation of the control rods performance placed in equilateral triangular arrangements in suppressing vortex induced vibration of a primary cylinder. The influence of the dimensionless parameters including attach angle α, spacing ratio G/D, and Reynolds number on the hydrodynamic forces of the primary cylinder is also investigated. The unsteady flow at Reynolds number of 200 and prandtl numbers of 0.7 and 7.0 is considered. In order to discretize the governing equations, a finite volume code based on the SIMPLEC algorithm is employed. Moreover, the local and mean Nusselt numbers are presented to illustrate the heat transfer characteristics of the primary cylinder and surrounding rods.

Keywords: Control rod; Vortex shedding; VIV suppression; Convection heat transfer; Overset grid

1. Introduction

Since the vortex shedding control from cylindrical bodies is an important subject in engineering situations, many flow control methods have been proposed in order to suppress fluctuations caused by the vortex shedding behind the cylinders. Obviously, lack of usage of active or passive flow control methods can lead to large strain and fatigue damage on these structures. The studies show that the large amplitude of the lift fluctuations and subsequently Vortex induced vibrations (VIV) of cylindrical bodies may be significantly reduced by using the control rods arranged near a main cylinder as a passive control method. On the other hand, vortex shedding as an unsteady flow structure can modify the pressure field on the cylinder surface and in turn enhances heat transfer. Indeed, heat transfer enhancement depends on the interaction among the wakes behind the bodies and the thermal boundary layers.

In addition to all of these, the grid generation around multiple bodies or complex geometries is an important problem and often involves many challenges. The overset grid method [1-5] employed in this research as an efficient technique provides the necessary flexibility to simulate the flow around a main cylinder attached by control rods. This approach involves constructing several structured grids that overlap with each other, while each grid can be changed independently from other grids. In the following, some of the published literatures in the field of flow around cylinders of equal and unequal diameter are reviewed.

Meneghini et al. [6] numerically investigated the shedding of vortices and flow interference between two circular cylinders with the same diameter in tandem and side-by-side configurations at Re = 100 and 200. They observed that in the tandem arrangement for $L > 3D$, the average drag coefficient of the downstream cylinder becomes positive and vortex shedding occurs from both cylinders. While a negative drag force was found for $L < 3D$ and vortex shedding was only observed for the downstream cylinder. Buyruk [7] carried out numerical analysis of the heat transfer for different cylinders configurations in cross flow of air. He studied effect of aspect ratio for two tandem cylinders with fixed Re = 400 and Pr = 0.7 and effect of Reynolds numbers for inline and staggered geometries. It was found that for tandem cylinders in the small gap, heat transfer rate on the downstream side of first cylinder and the upstream side of second cylinder was decreased due to the flow blockage by the second cylinder. Also, laminar boundary layer region heat transfer of the first cylinder was not affected by decreasing the ratio of L/D.

Lee et al. [8] investigated experimentally the effects of a control rod upstream on the drag characteristics and the wake structure behind the cylinder. The L/D ratio was between 1.5 and 4.0 for various rod diameters at Re = 2.0×10^4. They

*Corresponding author. Tel.: +98 8633663041
E-mail address: a-marjani@iau-arak.ac.ir
† Recommended by Associate Editor Shin Hyung Rhee

found that the control rod can be effective in the reduction of the hydrodynamic forces acting on the cylinder, as a maximum drag reduction about 25% for the cylinder with control rod was observed. Wang and Zhou [9] experimentally studied the vortex formation, interaction and evolution behind two side-by-side cylinders in the three different flow regimes. Special attention was paid to the asymmetrical flow regime of $1.2 < T/d < 2.0$, which was characterized by one narrow and one wide wake (T is the center-to-center cylinder spacing). It was found that the flow structure and its downstream evolution were closely linked to the phase relationship between the gap vortex in the wide wake and that in the narrow wake. Zhang et al. [10] studied numerically the mechanism of the formation and the convection of the vortices shedding from the cylinder with an upstream rod at low Reynolds numbers. Their results showed that the upstream rod can reduce the mean drag and the rms lift coefficients of the cylinder, especially in the cavity flow mode with the rod diameters $d/D = 0.3$ and 0.5.

Aerodynamic interference between two tandem cylinders of different diameters was studied experimentally by Alam et al. [11]. In their work, the downstream cylinder diameter, D, was fixed, while the upstream cylinder diameter, d, was varied between $0.24D$ and D. They observed that with decreasing d/D due to larger dynamic pressure between cylinders, the mean drag on the downstream cylinder increases. Furthermore, at very small d/D, the effect of upstream cylinder on the downstream cylinder wake was negligible, as the Strouhal number, mean drag and fluctuating drag and lift of the downstream cylinder approached to those of an isolated cylinder. Anagnostopoulos and Dikarou [12] performed numerical simulation of viscous oscillating flow past four circular cylinders for values of the frequency parameter equal to 50 and KC (Keulegan-Carpenter number) ranging from 0.2 to 10. They also assessed the mean transverse force acting on each cylinder, the rms values of the in-line and transverse forces and also the drag and inertia coefficients of the in-line force for each pitch ratio in the range of Keulegan-Carpenter numbers examined. Ambesi and Kleijn [13] investigated the effect of a single row of equidistantly and non-equidistantly spaced parallel cylindrical wires on forced convection heat transfer for Re of 0.001-600 and Pr of 0.7-10. They found that for equal open frontal area fractions, the Nusselt number in non-equidistant rows was lower than in equidistant rows for intermediate Reynolds numbers. While for very low and high Reynolds numbers, the uniformity of the inter-wire distance did not influence on the heat transfer rate.

Wang et al. [14] studied the flow past two tandem cylinders of different diameters at Re = 100 and 150. Their results indicated that although the existence of the upstream cylinder significantly can reduce the mean drag and rms lift coefficients of the main cylinder, its performance is dependent on the both ratios of d/D and G/D. In the other study performed by Wang et al. [15], the effect two small affiliated rotating cylinders on the drag and lift forces acting on the main cylinder as well as the heat transfer characteristics was investigated numerically. They found that the rotation direction of attached cylinders has great influence on the flow structure as well as the fluid forces of cylinder flow, as the co-current rotation can help suppress vortex shedding and reduce the drag and lift forces. Moreover, it was found that the average Nusselt number on the main cylinder with control increased with the rotation rate. Sufyan et al. [16] investigated the effect of Prandtl number along with rotation and also the effect of rotation under the influence of both the thermal boundary conditions (i.e. UHF and CWT) for the case of a cylinder and in the ranges of $0.7 \le \mathrm{Pr} \le 67$ and $5 \le \mathrm{Re} \le 40$. They found that heat transfer suppression occurs at intermediate and lower rotation rate and by increasing the rotation rate due to the increase in size of enveloping vortex, the heat transfer is decreased. Flow past a cylinder with multiple control rods was studied numerically by Zhu and Yao [17]. The range of the Reynolds numbers was from 1161.3 to 6387.1. The principle focus of this work was to assess VIV suppression efficacy of control rods located around a main cylinder using Computational fluid dynamics (CFD) models coupling with a Fuid-structure interaction (FSI) computational method. They found that although the increase of the number rod results in the reduction of the rms lift coefficient, it has the opposite effect on the mean drag coefficient and becomes larger.

In the present study, the characteristics of flow and forced convection heat transfer around a main cylinder attached by three control rods are investigated numerically at low Reynolds numbers. The overset grid approach is employed for constructing a rectangular background mesh and body-fitted meshes around $2D$ cylinders. The aim of this study is to assess the effects of applying three small rods located in equilateral triangular arrangements on the vortex shedding characteristics, hydrodynamic forces and heat transfer rate of a main cylinder.

2. Governing equations, geometry and numerical procedure

In Cartesian coordinate system, the dimensionless governing equations consist of continuity, momentum and energy equations for two-dimensional, unsteady, laminar, incompressible flow by constant properties assumption are given as follows:

$$\nabla . U = 0 \tag{1}$$

$$\frac{\partial U}{\partial t} + U.\nabla U = -\nabla P + \frac{1}{\mathrm{Re}}\nabla^2 U \tag{2}$$

$$\frac{\partial \theta}{\partial t} + U.\nabla \theta = -\nabla P + \frac{1}{\mathrm{Re}.\mathrm{Pr}}\nabla^2 \theta . \tag{3}$$

The dimensionless parameters are defined as:

$$x = \frac{x^*}{D},\ y = \frac{y^*}{D},\ u = \frac{U_x}{U_\infty},\ v = \frac{U_y}{U_\infty},\ P = \frac{P^*}{\rho U_\infty^2},$$
$$\theta = \frac{T - T_\infty}{T_w - T_\infty},\ t = \frac{U_\infty t^*}{D} \tag{4}$$

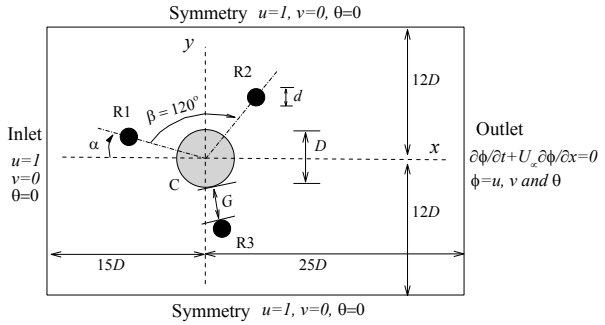

Fig. 1. Schematic diagram of the geometry considered and boundary conditions.

where D is the diameter of the cylinder, U is the flow velocity vector (U_x and U_y components in Cartesian coordinates), x* and y* are Cartesian coordinates, t^* is time, P^* is pressure, ρ is the density of the fluid, T is the temperature, θ is the dimensionless temperature and Tw is the cylinder wall temperature. Also, the Reynolds and Prandtl numbers are defined as Re (= $U_\infty D/\nu$) and Pr (= ν/a), where U_∞ is the free stream speed, ν and a are the kinematic viscosity and thermal diffusivity, respectively.

Fig. 1 shows the configuration sketch and boundary conditions applied in the present study. As observed the computational domain is a $40D \times 24D$ rectangular region and a main cylinder (denoted by C) attached by three control rods (denoted by R) in equilateral triangular arrangement are located in domain. G is the gap between the rod surface and the main cylinder surface and α is the angle between the negative x-axis and the central line connecting the cylinders of C and R1. Also, the angle interval of β is fixed at 120°. The cases including gap ratio $0.4 \le G/D \le 1.6$ and angle of attach (α) for a constant diameter ratio of $d/D = 0.24$ are investigated in this study. The boundary conditions used are also specified in Fig. 1 and can be summarized as follows:

For the major grid boundaries; the uniform flow and constant temperature are applied at the inlet boundary. The top and bottom boundaries are assumed to be far enough from the cylinder surface and the symmetry boundary condition is used. At the outlet boundary, the Convective boundary condition (CBC) is satisfied with the fully-developed flow assumption.

For the minor grid boundaries; at the cylinder surface, no-slip condition with constant wall temperature is imposed. Some dimensionless parameters required in computations including the drag and lift coefficients (C_D, C_L), the Strouhal number (St), local and mean Nusselt numbers (Nu_L, Nu) are defined as follows:

$$C_D = \frac{2F_D}{\rho U_\infty^2 D}, \quad C_L = \frac{2F_L}{\rho U_\infty^2 D}, \tag{5, 6}$$

$$\mathrm{Nu}_L = \frac{h_L.D}{k}, \quad -k\frac{\partial T}{\partial n}\bigg|_W = h_L\left(T_W - T_\infty\right), \tag{7, 8}$$

$$Nu = \frac{1}{2\pi}\int_0^{2\pi} Nu_L dL, \quad St = \frac{f.D}{U_\infty} \tag{9, 10}$$

Table 1. Validation of numerical model and grid independence study for an isolated cylinder at Re = 200.

References			C_D^M		C_L^A	St	Nu1 pr = 0.7	Nu2 Pr = 7.0
Liu et al. [19]			1.31±0.049		0.69	0.192	-	-
Hilpert and Forsch [20]*			-		-	-	7.162	15.431
Churchill and Bernstein [21]			1.25		-	0.196	7.188	16.642
Ding et al. [22]			1.348±0.05		0.659	0.196	-	-
Present work	H-grid size	O-grid size	Δt	C_D^M	C_L^A	St	Nu pr = 0.7	Nu Pr = 7.0
Case 1	330×230	150×120	0.01	1.339	0.665	0.194	7.106	16.363
Case 2	230×130	95×65	0.01	1.327	0.649	0.191	7.111	16.461
Case 3	410×310	210×180	0.01	1.344	0.680	0.195	7.005	16.281
Case 4	330×230	150×120	0.02	1.334	0.654	0.192	7.091	16.201

*Experimental

where F_D and F_L denote the drag and lift forces, respectively. f is the frequency of vortex shedding, h_L is the local heat transfer coefficient, k is the thermal conductivity of the fluid and n is the direction normal to the cylinder.

In this study, a finite volume code based on the SIMPLEC algorithm together with a collocated variable arrangement is developed for the numerical solution. A second order accurate Crank-Nicolson scheme is employed for time integration and the convective terms are solved using the QUICK discretization scheme. The pressure-velocity coupling is made by the Rhie-Chow algorithm [18]. In addition, the overset grid method is applied to distribute the grid points over the whole domain around the main cylinder and rods. The concerning of this method is constructed several structured grids (minor and major grids) and each grid can be changed separately from other grids. In the present work, hole points are situated inside the solid surface of the cylinders. As regards each cylinder has its own grid, the hole points are also defined in regions where the grid overlaps solid cylinders belonging to the other grids. It should be noted that an interpolation algorithm and a search algorithm are used to transfer the information between grids.

3. Grid independence and validity checking

A test of grid independence is conducted in order to ensure the accuracy of the computational approach. The results of flow around an isothermal cylinder at Re = 200 and Pr = 0.7 and 7.0 are presented and then compared with other experimental and numerical studies in Table 1. In general, it can be clearly found from Table 1 that the governing non-dimensional parameters indicate the good agreement with the other literatures for the all cases, nevertheless it seems case 1 is a more appropriate selection. After the validation of the numerical model, flow around a primary cylinder attached by three control rods located in equilateral triangular arrangements is simulated. Fig. 2 shows the meshes used for this study.

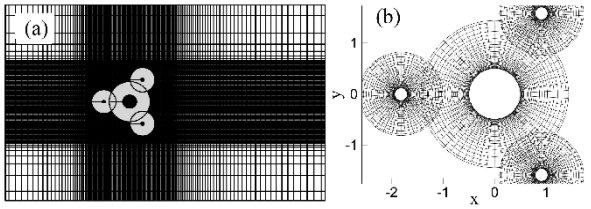

Fig. 2. Overset grids: (a) Whole domain composed of minor and major grids; (b) minor grid around the cylinders.

4. Results

4.1 Force coefficient

The mean drag and root mean square lift coefficients of the main cylinder versus spacing ratio G/D for three attach angles of $\alpha = 0°$, 30° and 60° at Re = 200 and $d/D = 0.24$ are plotted in Fig. 3. As observed the drag and lift coefficients strongly depend on the attach angle α, while the variations of the drag coefficients with spacing ratio are relatively smaller than those of the lift coefficients. It can be seen from Fig. 3(a) that the overall trend of the variations of the mean drag coefficients for three attach angles considered is nearly similar, although the minimum drag force at $\alpha = 30°$ occurs in the middle value of the spacing ratio i.e., $G/D = 1.0$, while for other two angles of $\alpha = 0°$ and $\alpha = 60°$ its minimum is seen in the large spacing ratio of $G/D = 1.6$. It should be noted that in general, the drag coefficients mostly decrease by increasing the spacing ratio from 0.4 to 1.6. The maximum drag forces appear at $\alpha = 60°$, as at the largest spacing ratio of $G/D = 1.6$ where the drag force reaches to its minimum value at this angle, it drops only about 13.06% relative to that of a single cylinder (1.339 as presented in Table 1). While the minimum drag forces locate at $\alpha = 0°$ and the corresponding drag coefficient at $G/D = 1.6$ is significantly smaller than that of a single cylinder (about 40.5% reduction).

In the range of $0.4 \leq G/D \leq 1.6$ and at $\alpha = 60°$, the maximum drag coefficient belongs to the spacing ratio $G/D = 0.4$, where shows a slight decrease in the mean drag coefficients (about 1.5%) as compared with that of a single cylinder.

On the contrary to the drag coefficients, the overall trend of the variations of the lift coefficients is incremental with respect to increasing the spacing ratio (see Fig. 3(b)). Exceptions are clearly observed at $\alpha = 30°$ and $\alpha = 60°$. For $\alpha = 60°$, a significant reduction occurs in the lift coefficients as the increase of the spacing ratio from 0.4 to 0.6. For $\alpha = 30°$, on increasing the spacing ratio from $G/D = 0.4$ to 1.0 the lift coefficients decrease and reach to their minimum, then with the further increase of the spacing ratio to 1.4, these coefficients drastically increase and achieve their maximum values at $G/D = 1.4$, where nevertheless is about 64% less than that a single cylinder (i.e., 0.47). However from three attach angles considered, the minimum lift coefficients are observed at $\alpha = 60°$ in the range of $0.8 \leq G/D \leq 1.0$, but it seems in general the control rods arranged at $\alpha = 0°$ have more performance in suppressing the mean drag and rms lift forces of the main cylinder.

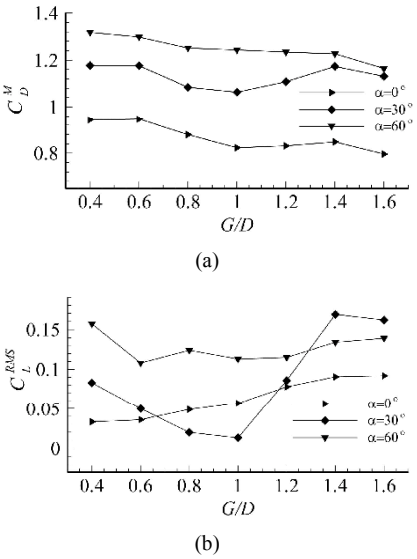

Fig. 3. Variations of force coefficients with spacing ratio G/D at three attach angles of $\alpha = 0°$, 30° and 60°, Re = 200 and $d/D = 0.24$: (a) Mean drag coefficients; (b) RMS lift coefficients.

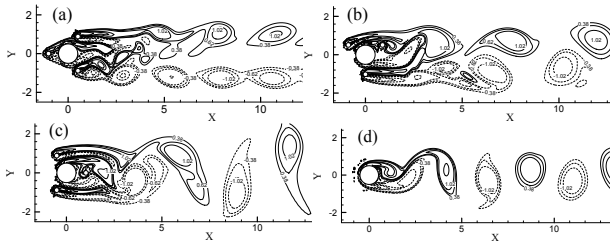

Fig. 4. Vorticity contours behind the cylinder group for $G/D = 0.4$ with different attach angles of (a) $\alpha = 0°$; (b) $\alpha = 30°$; (c) $\alpha = 60°$ at Re = 200 and d/D = 0.24; (d) vorticity contour behind a single cylinder at Re = 200.

Furthermore, in comparison with studies that employed one or two control rods [14, 23], the coefficients obtained for three control rods at $\alpha = 0°$ show a greater reduction. As for example in the study of Zhou et al. [23] that two tripping rods were used, the maximum reduction of the drag coefficient at the optimum angular position (i.e., $\alpha = 40°$) was about 18% for Re = 200. Also as will become clear later, the lift coefficients presented in this study for Re = 100 and $\alpha = 0°$ are very smaller than those of reported by Wang et al. [14] for $d/D = 0.3$ (closer to $d/D = 0.24$).

4.2 Flow patterns and characteristics of vortex shedding

Fig. 4 presents the instantaneous vorticity contours behind the cylinder group at small spacing ratio of $G/D = 0.4$ with different attach angles ($\alpha = 0°$, 30° and 60°) and dimensionless time of $t = 300$. The solid and dashed lines are respectively employed to identify the vortices with positive and negative signs. According to Fig. 4(a), the small rod R1 is attached at the upstream of the main cylinder and two other small rods (R2 and R3) in side-by-side arrangement are located at the

downstream of the main cylinder.

It can be found from figure that for the small spacing ratio of 0.4 at α = 0°, the proximity effect is weak and the flow passing through the gap among the cylinders is developed as two separate vortex street regions in the far wake. Although in this case, in the near wake region, a relatively weak interaction is observed between the positive vortices generated from the upper sides of the control rods R2 and R3 which slightly deflects the wake flows of the main cylinder and rod R1 to the top side. Compared with the other two attach angles (α = 30°, 60°), the relative stability of the wake flows behind the main cylinder can cause reduction of fluctuating lift force exerted on the main cylinder.

Fig. 5 shows the pressure contours and the streamlines around the main cylinder with and without control rod. As expected, for the cylinder attached by control rods at α = 0°, the separation points move further rear (Figs. 5(a) and (b)). Obviously, the upstream rod R1 and two rods of the downstream (R2 and R3) play the dominant role in the separation point displacement on the surface of the main cylinder. As can be confirmed from figure, two side-by-side rods induce the necking of the streamlines toward the rear surface of the main cylinder and the separation occurs later in comparison with the case without the control rod. Consequently, the higher pressure distribution behind the main cylinder which is located among three control rods can lead to reduction of the pressure difference between the upstream and downstream sides of the main cylinder. Due to the existence of the control rod R1, the reduction of stagnation pressure on the upstream of the main cylinder is also expected. All of these can justify the considerable reduction of drag force acting on the main cylinder at α = 0°.

In Fig. 4(b) as shown, at α = 30° the main cylinder is attached by two rods arranged in tandem (R1 and R2) and also the rod R3 which is placed under the main cylinder. As can be seen, the positive vortices shed from the upper sides of the cylinders R1, R2 and C are merged together and then interact with the positive vortices generated from the rod R3, clearly making the large positive vortices at the upper row of the vortex street observed. Simultaneously, the interactions between the negative vortices shed from the cylinders R3 and C result in the formation of the lower row of the vortex street. On the contrary, the negative vortices generated from the rods R1 and R2 are weak and almost disappeared. In this case it should be noted that although similar to α = 0°, two separate vortex street rows are observed, but the size of vortices and the distance between them is increased which results in increasing the flow instability. In the middle region, the vortex shedding behind the main cylinder is striking relative to α = 0°. Moreover, the in-phase synchronized vortex shedding from the rods R1 and R2 is detected that have a negligible phase difference with cylinder C, resulting in larger lift force on the main cylinder.

Fig. 5(c) shows the streamlines around the main cylinder with control rod at α = 30°. Obviously, moving the separation

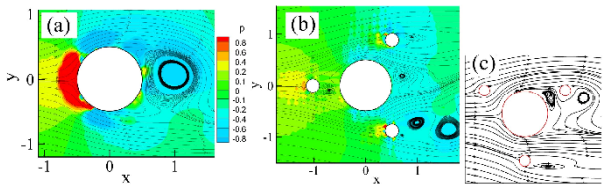

Fig. 5. (a) Pressure distribution and streamline around a single cylinder; (b) pressure distribution and streamline around the main cylinder attached by the rods at α = 0°, G/D = 0.4 and Re = 200; (c) streamline around the cylinders at α = 30°, G/D = 0.4 and Re = 200.

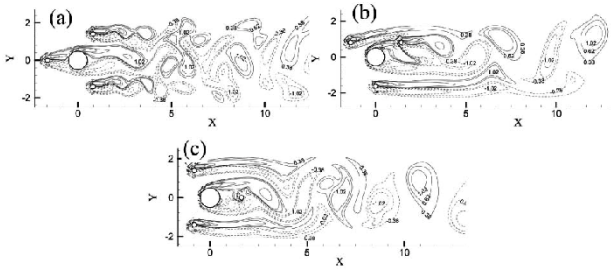

Fig. 6. Vorticity contours behind the cylinder group for G/D = 1.0 with different attach angles at Re = 200: (a) α = 0°; (b) α = 30°; (c) α = 60°.

points on the rear surface of the main cylinder is reduced, especially on its upper surface due to the asymmetrical arrangement of the control rods with respect to the flow direction. Eventually, the higher pressure distribution on the lower side of the main cylinder leads to lift larger force. Furthermore, the higher pressure in the stagnation point region of the main cylinder strictly increases the drag force compared with α = 0°. At α = 60° (see Fig. 4(c)), the proximity effect is strengthened and the alternative vortex shedding of van Karman vortices is observed. Although, the size of vortices and the period of their shedding are increased relative to an isolated cylinder, but the large vortices shed from the cylinder group in the further distance. Certainly, the lower pressure distribution behind the main cylinder is expected than that in α = 30°.

Fig. 6 plots the instantaneous vorticity contours around the cylinder group at the spacing ratio of G/D = 1.0 for the attach angles considered. As found from the comparison between Fig. 6(a) and 4(a), at α = 0° by increasing the spacing ratio from G/D = 0.4 to 1.0, the near wake flows behind the middle row of the main cylinder are developed while the vortex shedding from the small rod R2 and R3 is weakened. The interactions among three rows of the vortex street shed from the cylinders of R1 and C, R2 and R3 generate the diagonal vortices scattered in the far wake and thereby the flow structure becomes more unstable compared to G/D = 0.4. At the larger spacing ratio G/D = 1.0, the effect of the control rod R1 on the reduction of the drag force is more significant due to the lower pressure distribution in the upstream of the main cylinder.

In Fig. 6(b), at α = 30° the vortex shedding in the near wake of the rods R1 and R3 is suppressed and the vortices shed from cylinders of C and R2 interact with the wake of these rods (R1 and R3) at far downstream. Also, the vortex shed-

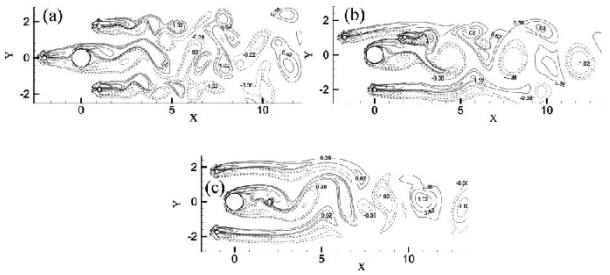

Fig. 7. Vorticity contours behind the cylinder group for G/D = 1.4 with different attach angles at Re = 200: (a) α = 0°; (b) α = 30°; (c) α = 60°.

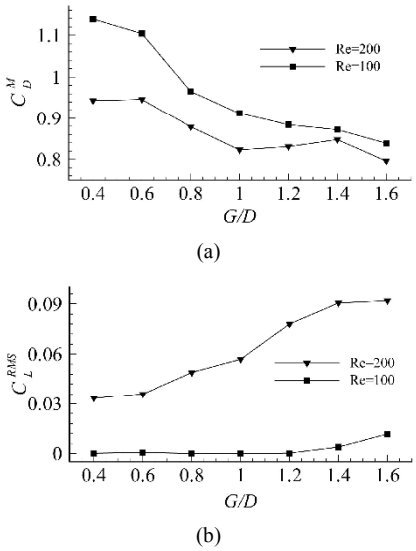

Fig. 8. Variations of force coefficients with G/D for Re = 100 and 200 at attach angle α = 0°: (a) Mean drag coefficient; (b) RMS lift coefficient.

ding behind the main cylinder takes place downstream further, leading to a significant reduction of lift force, even less than its value at α = 0°. Due to the presence of the control rod R1 at more upstream relative to G/D = 0.4, the lower distribution on the upstream side of the main cylinder is expected and this can be effective in the reduction of the drag coefficient.

For α = 60° on increasing the spacing ratio from G/D = 0.4 to G/D = 1.0, the proximity effect is weakened (Fig. 6(c)), and the size of vortex and the period of vortex shedding is decreased. Furthermore, the relative stability in the near wake of the cylinder group compared with Fig. 4(c) can account for the reduction of fluctuating lift acting on the main cylinder. With further increasing of the spacing ratio to 1.4, for α = 0° and α = 60° no significant change in the flow structure behind the cylinder group is found (see Fig. 7), for instance at α = 0° instability and scattering of the vortices shed are partially increased. But at α = 30° (Fig. 7(b)), the vortex shedding in the near wake of the main cylinder and the relatively strong interaction of vortices generated from the group cylinder are striking.

The variations of mean drag and rms lift coefficients of the main cylinder with spacing ratio G/D at two Reynolds numbers of 100 and 200 and attach angle α = 0° are shown in Fig. 8. As observed, the drag and lift coefficients depend strongly on the Reynolds number, although for the mean drag coefficients this dependence is decreased under the large spacing ratios. Evidently, by changing the Reynolds number to 100, the viscous effects in the boundary layers surrounding the cylinders become more significant as the spacing ratio decreases. Unlike the drag coefficients, the lift coefficients of the main cylinder at Re = 100 are smaller than those at Re = 200, as more these coefficients remain very close to zero or zero and only at the large spacing ratios slightly increase. While the rms lift coefficients obtained by Wang et al. [14] for different spacing ratios at d/D = 0.3 (closer to d/D = 0.24) and Re = 100 are about 0.1 and higher.

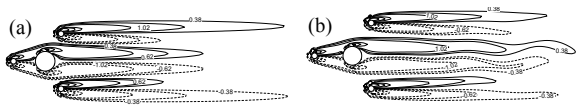

Fig. 9. Comparison of the vorticity contours around the cylinders for different spacing ratios at Re = 200 and α = 0°: (a) G/D = 1.0; (b) G/D = 1.4.

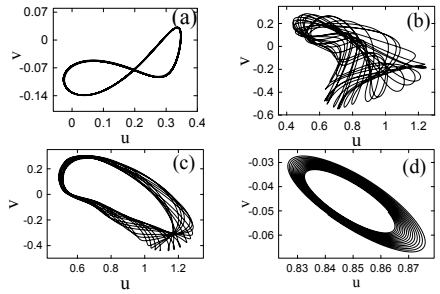

Fig. 10. Phase diagrams for different spacing ratios at α = 0°: (a) G/D = 0.4, Re = 200; (b) G/D = 1.0, Re = 200; (c) G/D = 1.4, Re = 200; (d) G/D = 1.4, Re = 100.

Fig. 9 shows the vorticity contours behind the cylinder group for two spacing ratios of G/D = 1.0 and 1.4 at Re = 100 and attach angle α = 0°. As can be seen from Fig. 9(a), the flow structure is fully symmetric and stable at G/D = 1.0 and no vortex shedding occurs in the wake. Clearly, in such a state the lift coefficients tend to zero. Although by further increasing the spacing ratio to 1.4, the symmetry of the flow structure is somewhat destroyed and thereby the lift coefficients slightly increase.

The phase diagrams for different spacing ratios are displayed in Fig. 10. Phase diagrams are constructed by plotting the stream-wise velocity component against the transverse velocity component at a sampling location 3D downstream from the centre of the main cylinder [24]. According to Fig. 10, a single orbit is observed for the spacing ratio of 0.4 at Re = 200 that reflects the periodic behavior of the flow. With increase of the spacing ratio from 0.4 to 1.6, the flow periodicity is lost and the irregular orbits appear. Furthermore at Re = 100, the irregular orbits only are observed for the large spacing ratio of 1.4 and 1.6.

Table 2. The mean Nusselt number for the cylinders at Re = 200.

G/D	Pr = 0.7				Pr = 7.0			
	Nu_C	Nu_{R1}	Nu_{R2}	Nu_{R3}	Nu_C	Nu_{R1}	Nu_{R2}	Nu_{R3}
0.4	4.917	2.931	3.661	3.486	11.372	6.566	8.798	8.024
0.8	4.814	3.128	3.652	3.629	11.434	6.822	8.290	8.245
1.0	4.821	3.164	3.669	3.700	11.409	7.018	8.357	8.342
1.4	4.885	3.264	3.609	3.619	11.522	7.317	8.146	8.099
1.6	4.929	3.280	3.617	3.672	12.027	7.447	8.184	8.289

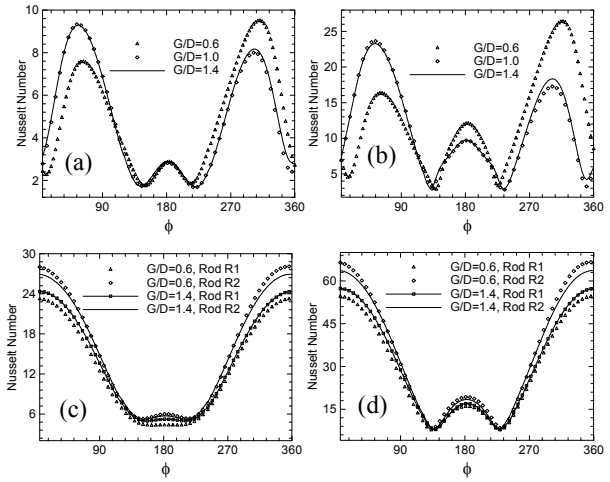

Fig. 11. The local number Nusselt distributions on the surface of the cylinders for different spacing ratios at Re = 200, α = 0° and Pr = 0.7 (a) and (c); Pr = 7.0 (b) and (d).

4.3 Heat transfer results

The local Nusselt numbers on the surface of the main cylinder and rods for different spacing ratios at the attach angle of α = 0° and Re = 200 are shown in Fig. 11. As can be seen, the local Nusselt number distribution along the main cylinder surface for the spacing ratios considered is asymmetric while for the rods of R1 and R2, a symmetric distribution of Nusselt number is observed. This indicates that the gradient of the heat transfer rate versus φ for the main cylinder is significantly different relative to small rods (φ is the angular displacement from the forward stagnation point). The maximum local Nusselt number on the main cylinder surface appears in the regions $\varphi \approx 60°$ and also $\varphi \approx 300°$, where the thickness of the boundary layer is smallest. While the minimum local Nusselt number occurs at the upstream stagnation point (φ = 0°) and also the regions of $\varphi \approx 130°$ and $\varphi \approx 230°$ (Figs. 11(a) and (b)). For the rods R1 and R2, the maximum local Nusselt number is observed at the upstream stagnation point. Evidently, it is found that by increasing the Prandtl number from 0.7 to 7.0 the value of local Nusselt number on the surface of the main cylinder and rods increases.

Table 2 presents the mean Nusselt numbers for the main cylinder (Nu_C) and small rods ($Nu_{R1\text{-}R3}$) for different spacing ratios at Re = 200 and Pr = 0.7 and 7.0. The mean Nusselt number is computed by numerical integration from the local Nusselt number along the surface of the cylinders. As is confirmed from figure, the mean Nusselt number depends on the Prandtl number and then spacing ratio *G/D*. Compared with a single cylinder, a considerable reduction in heat transfer of the main cylinder is observed that by decreasing the spacing ratio becomes more evident (about 35% reduction). The minimum mean Nusselt numbers is obtained for the small rod R1, influencing by the thermal wake of the main cylinder.

4.4 Conclusions

In the present work, the two dimensional simulation of fluid flow and forced convection heat transfer from a main cylinder attached by three control rods at Re = 200 is performed using the overset grid method. The control rods are configured in equilateral triangular arrangements around the main cylinder. The influence different parameter of the problem as the spacing ratio *G/D*, angle of attach α and Reynolds number on the time averaged drag and rms lift coefficients of the main cylinder and vortex shedding characteristics of the cylinder group is investigated. The results indicate that for Re = 200 and the range of $0.4 \leq G/D \leq 1.6$, the efficiency of control rods in suppressing the vortex shedding behind the main cylinder is increased at α = 0° compared with the other two attach angles (α = 30° and α = 60°). As at α = 0°, the drag and lift coefficients of the main cylinder attached by rods are respectively about 50% and 90% less relative to an isolated cylinder.

The evaluation of the phase diagrams reveals that at Re = 200 the flow periodicity is diminished for $G/D > 0.4$, while for Re = 100 the irregular orbits are appeared at *G/D* = 1.4 and 1.6. Furthermore, in this study the results of the heat transfer are presented by the local and mean Nusselt numbers for different spacing ratios at α = 0°, Re = 200 and Pr = 0.7 and 7.0. It is found that the gradient of the heat transfer rate versus angular displacement (φ) for the main cylinder differs significantly relative to small rods and a asymmetric distribution of Nusselt number around the main cylinder is predicted. Relative to single cylinder, a sensible reduction in the mean Nusselt number of the main cylinder is also observed that at smaller spacing ratios this tendency becomes clearer. The capability of the overset grid approach to accurately predict the efficiency of the control rods is demonstrated.

References

[1] H. S. Tang, S. C. Jones and F. Sotiropoulos, An overset-grid method for 3D unsteady incompressible flows, *Journal of Computational Physics,* 191 (2003) 567-600.

[2] J. Cai, H. M. Tsai and F. Liu, A parallel viscous flow solver on multi-block overset grids, *Computers & Fluids*, 35 (2006) 1290-1301.

[3] J. Cai, H. M. Tsai and F. Liu, Numerical simulation of vertical flows in the near field of jets from notched circular nozzles, *Computers & Fluids*, 39 (2010) 539-552.

[4] G. Wang, F. Duchaine, D. Papadogiannis, I. Duran, S. Moreau and Y. M. L. Gicquel, An overset grid method for large eddy simulation of turbo machinery stages, *Journal of Computational Physics*, 274 (2014) 333-355.

[5] T. T. Tran and D. H. Kim, The aerodynamic interference effects of a floating offshore wind turbine experiencing platform pitching and yawing motions, *Journal of Mechanical Science and Technology*, 29 (2) (2015) 549-561.

[6] J. R. Meneghini, F. Saltara, C. L. R. Siqueira and J. A. Ferrari Jr., Numerical simulation of flow interference between two circular cylinders in tandem and side-by-side arrangements, *Journal of Fluids and Structures,* 15 (2001) 327-350.

[7] E. Buyruk, Numerical study of heat transfer characteristics on tandem cylinders, inline and staggered tube bank in cross-flow of air, *International Communications in Heat and Mass Transfer,* 29 (3) (2002) 355-366.

[8] S. J. Lee, S. I. Lee and C. W. Park, Reducing the drag on a circular cylinder by upstream installation of a small control rod, *Fluid Dynamics Research*, 34 (2004) 233-250.

[9] Z. J. Wang and Y. Zhou, Vortex interactions in a two side-by-side cylinder near-wake, *International Journal of Heat and Fluid Flow,* 26 (2005) 362-377.

[10] P. F. Zhang, J. J. Wang and L. X. Huang, Numerical simulation of flow around cylinder with an upstream rod in tandem at low Reynolds numbers, *Applied Ocean Research*, 28 (2006) 183-192.

[11] M. M. Alam and Y. Zhou, Strouhal numbers, forces and flow structures around two tandem cylinders of different diameters, *Journal of Fluids and Structure*, 24 (2008) 505-526.

[12] P. Anagnostopoulos and Ch. Dikarou, Numerical simulation of viscous oscillatory flow past four cylinders in square arrangement, *Journal of Fluids and Structures,* 27 (2011) 212-232.

[13] D. Ambesi and C. R. Kleijn, Laminar forced convection heat transfer to ordered and disordered single rows of cylinders, *International Journal of Heat and Mass Transfer,* 55 (2012) 6170-6180.

[14] Y. T. Wang, Z. M. Yan and H. M. Wang, Numerical simulation of low-Reynolds number flows past two tandem cylinders of different diameters, *Water Science and Engineering*, 6 (4) (2013) 433-445.

[15] J. S. Wang, Y. X. Xu and Y. S. Tian, Active control of circular cylinder flow by affiliated rotating cylinders, *Science China Technological Sciences*, 56 (5) (2013) 1186-1197.

[16] M. Sufyan, S. Manzoor and N. A. Sheikh, Free stream flow and forced convection heat transfer across rotating circular cylinder in steady regime: effects of rotation, Prandtl number and thermal boundary condition, *Journal of Mechanical Science and Technology*, 29 (4) (2015) 1781-1797.

[17] H. Zhu and J. Yao, Numerical evaluation of passive control of VIV by small control rods, *Applied Ocean Research,* 51 (2015) 93-116.

[18] C. M. Rhie and W. L. Chow, Numerical study of the turbulent flow past an airfoil with trailing edge separation, *AIAA Journal,* 21 (11) (1983) 1525-1532.

[19] C. Liu, X. Zheng and C. H. Sung, Preconditioned multigrid methods for unsteady incompressible flows, *Journal of Computational Physics,* 139 (1998) 35-57.

[20] R. Hilpert and Geb. Forsch, Heat Transfer from Cylinders, *Ingenieurwes,* 4 (1933) 215.

[21] S. W. Churchill and M. J. Bernstein, A correlating equation for forced convection from gases and liquids to a circular cylinder in cross flow, *Journal of Heat Transfer,* 99 (1977) 300-306.

[22] H. Ding, C. Shu, K. S. Yeo and D. Xu, Numerical simulation of flows around two circular cylinders by mesh-free least square-based finite difference methods, *International Journal for Numerical Methods in Fluids,* 53 (2007) 305-332.

[23] C. Y. Zhou, L. Wang and W. Huang, Numerical study of fluid force reduction on a circular cylinder using tripping rods, *Journal of Mechanical Science and Technology*, 21 (2007) 1425-1434.

[24] G. Biswas and S. Sarkar, Effect of thermal buoyancy on vortex shedding past a circular cylinder in cross-flow at low Reynolds numbers, *International Journal of Heat and Mass Transfer*, 52 (2009) 1897-1912.

Somayeh Harimi is currently Ph.D. student at Department of Applied Chemistry, Arak Branch, Islamic Azad University, Arak, Iran. She has interest in research on topics such as computational fluid dynamics, flow control and heat transfer (Somayehharimi@gmail.com).